Geoderma 347 (2019) 90–102

Contents lists available at ScienceDirect

Geoderma

journal homepage: www.elsevier.com/locate/geoderma

Determining the influence of catchment area on intensity of gully erosion using high-resolution aerial imagery: A 40-year case study from the Loess Plateau, northern China

Shengtian Yang[a,d], Yabing Guan[b], Changsen Zhao[a,e,*], Chunbin Zhang[b], Juan Bai[b], Ke Chen[c]

[a] College of Water Sciences, Beijing Normal University, Beijing Key Laboratory of Urban Hydrological Cycle and Sponge City Technology, Beijing 100875, China
[b] State Key Laboratory of Remote Sensing Science, Faculty of Geographical Science, Beijing Normal University, Beijing Key Laboratory for Remote Sensing of Environment and Digital Cities, Beijing 100875, China
[c] School of Tourism Culture and Geography, Huanggang Normal University, Hubei 438000, China
[d] School of Geography and Environmental Science, Guizhou Normal University, Guiyang 550001, China
[e] ICube, UdS, CNRS (UMR 7357), 300 Bld Sebastien Brant, CS 10413, 67412 Illkirch, France

ARTICLE INFO

Handling Editor: Yvan Capowiez

Keywords:
Gully erosion
Aerial photography
UAV remote sensing
Catchment area
Loess Plateau
China

ABSTRACT

Gully erosion can be a serious threat to ecologic and socio-economic stability. Although gully erosion intensity is highly impacted by catchment area changes, few studies have focused on the relevant mechanisms. This study presents a new approach to studying this issue by combining historic aerial photography and recent unmanned aerial vehicle (UAV) imagery to determine changes in gully morphology over 40 years on China's Loess Plateau, one of the world's most erosion-prone regions. Aerial photographs from 1976 were matched with UAV imagery taken in 2017 to compare gully and surface conditions in two study areas over time. Next, a new method was developed for calculating changes in gully volume and erosion moduli based on the UAV-derived digital surface model. Finally, the impacts of catchment area change on gully erosion moduli over the study period were analyzed. The results showed that the catchment areas decreased by 0.71–77.88%; greater decreases resulted in lower gully erosion moduli (with an exponential correlation) and reducing catchment area effectively slowed gully development. In addition, regional agricultural terrace construction has reduced the catchment areas, in turn reducing the amount of runoff entering gullies and thus reducing incision. Therefore, the management and maintenance of abandoned terraces should be strengthened by local governments and stakeholders to reduce runoff-induced gully erosion and sediment loss from upslope areas. The methodologies and results of this study have the potential to provide significant scientific references for the conservation of runoff and sediment in erosion-prone regions of China and elsewhere.

1. Introduction

Gullies have been defined as channels whose width and depth do not allow for normal tillage (Wu and Cheng, 2005). Gullies should be considered as complex geomorphic systems which are induced and transformed not only by overland flow, but also by subsurface processes (such as soil piping) and mass movements (Bernatek-Jakiel and Poesen, 2018; Poesen et al., 2003; Selkimäki and González-Olabarria, 2017). The initiation and development of gullies can lead to many socio-economic problems including damage to agricultural production, farmland, and residential land (Huang et al., 2012). It is particularly important to recognize and monitor gully development in order to mitigate or control the subsequent effects. Monitoring parameters can include gully head retreat distance, expansion area, and volume change. However, as the first two factors are two-dimensional, they do not adequately reflect the development of gully incision. In contrast, volume change (a three-dimensional factor) is more capable of accurately reflecting total erosion, so is widely used in gully erosion monitoring (Marzolff and Poesen, 2009; Peter et al., 2014; Stöcker et al., 2015; Wu et al., 2008).

Catchment area is another critical factor in gully erosion assessment (Xu et al., 2017), and is the most important variable explaining linear,

Abbreviations: AEA, average end area; DOM, digital orthophoto map; DSM, digital surface model; TLS, terrestrial laser scanning; UAV, unmanned aerial vehicle

* Corresponding author.
E-mail addresses: yangshengtian@bnu.edu.cn (S. Yang), guanyabing@mail.bnu.edu.cn (Y. Guan), zhaochangsen@bnu.edu.cn (C. Zhao), chenkebj2000@sina.com.cn (K. Chen).

https://doi.org/10.1016/j.geoderma.2019.03.042
Received 30 June 2018; Received in revised form 30 January 2019; Accepted 24 March 2019

areal, and volumetric gully headcut retreats over medium to long periods of time (Frankl et al., 2012). Patton and Schumm (1975) first discovered the threshold phenomenon of gully formation, demonstrating an inverse relationship between catchment area and critical slope. Vandaele et al. (1996) further established a power function relationship between upslope catchment area and critical slope. Based on these studies, Cheng et al. (2007) determined the power function parameter values of this critical topographic relationship through field investigation. Such previous studies were primarily focused on the relationship between topography and gully formation, with less emphases on the impact of catchment area; this exclusion has hindered a comprehensive understanding of gully development.

Sinkhole has been observed in both natural and anthropogenic landscapes, in a wide range of climatological, geomorphological and pedological settings (Verachtert et al., 2010). Sinkhole leads to directly soil loss and is recognized as an important reason for the development of gullies (Frankl et al., 2012). It may lead to new gully formation after total pipe collapse as well as it may deepen or widen the existing gully channels or contribute to gully head retreat (Bernatek-Jakiel and Poesen, 2018). Sinkholes are widely distributed on the Loess Plateau (Peng et al., 2007; Peng et al., 2018). Previous studies mainly focused on the classification, distribution and formation of sinkhole (Wang, 1989; Zhu, 1958), as well as hydrological process and sediment concentration of sinkhole flow (Zhu, 1997; Zhu et al., 2002). However, soil loss due to sinkhole is often overlooked in gully erosion studies and may result in underestimated erosion rates (Bernatek-Jakiel and Poesen, 2018).

Monitoring changes in both gully volume and catchment area are thus key experimental methods for analyzing factors that influence the relevant erosive processes, though the former is more complicated. Remote sensing data and ground observation are commonly used for this purpose, with the latter encompassing three primary methods. First, erosion marker pins were widely used in early studies, but this method is time-consuming and laborious with relatively low accuracy and serious practical limitations in larger monitoring areas (Wu et al., 2008). Second, Global Positioning System (GPS) technology allows a digital terrain model of affected regions to be developed by spatial interpolation of numerous GPS sample points containing coordinate and elevation information (Hu et al., 2007; Wu and Cheng, 2005). However, this method requires large number of densely ground-sampled points (e.g., 5574 points within 0.0865 km^2 (Wu and Cheng, 2005)), which can cause practical limitations. Third, ground-based terrestrial laser scanning (TLS) technology can obtain high-resolution digital terrain models of erosive areas and identify gully characteristics and depositional distribution at different times, thus overcoming the primary dense-sampling limitation of GPS-sourced terrain models. However, this method requires more specialized expertise with regard to deploying a medium-range scanner for measurements of large spatial objects and coding a pattern of normalized, black and white target shields (Kociuba et al., 2015). In addition, TLS surveys are more costly (particularly when time-series data are required) and are more limited by range and line of sight, making them harder to apply over large areas (Glendell et al., 2017).

In comparison, satellite or aerial remote sensing data allow the comparison of multiple images at different times to detect surface changes, evaluate gully development, and effectively solve many of the challenges posed by ground observation. Satellite remote sensing can be used to extract the morphological characteristics of a gully from imagery and estimate changes in gully volume using measurements of length, width, and area (Li et al., 2017b). However, it remains difficult to achieve accurate results using this method due to the limited spatial resolution of satellite imagery. In comparison, aerial photography uses optical photographic technologies to acquire stereopair images of gullies from a stable platform at a certain height. The resulting high-precision digital surface models (DSMs) can directly estimate changes in gully volume (Marzolff and Poesen, 2009; Murray et al., 2013). The most commonly used aerial photography platforms include manned aircraft (Ries, 2010; Ries and Marzolff, 2003) and the rapidly developing field of unmanned aerial vehicles (UAVs) (d'Oleire-Oltmanns et al., 2012; Eltner et al., 2015). The shortcomings of previous methods have encouraged the development of high-precision, low-cost aerial photography as the best method for gully erosion monitoring, especially as this is less dependent on specialized expertise.

Gully development is particularly likely in loess soil due to its unconsolidated nature (Muhs, 2018). Loess-type deposits cover up to 10% of the Earth's surface, most commonly in central Asia, central Europe, the Ukraine, Argentina, and North America (Tsoar, 1987), while the most widely distributed region is the Loess Plateau in China (Xin et al., 2011; Zhao et al., 2013). Loess sediments in this region have been transported from adjacent deserts in central Asia and Mongolia by prevailing westerly winds and deposited as a plateau (Amit et al., 2013; Sun, 2002). Gully erosion in the Loess Plateau is extremely active, serving as the main source of erosive sediment production in the area's small watersheds and contributing ~60–90% of the area's total sediment yield (Liu et al., 2012). Approximately 60% of the land in this region suffers from soil erosion (Shi and Shao, 2000), with a modulus as high as 15,000 $t\,km^{-2}\,a^{-1}$, with ~91,200 km^2 subject to a soil erosion rate of over 8000 $t\,km^{-2}\,a^{-1}$ (Li et al., 2017a). Such erosion leads to serious problems including the loss of soil organic matter and nutrients (Fu et al., 2004) and the degradation of soil physical properties (Wang and Shao, 2013). The Loess Plateau is among the most erosion-affected regions in the world, along with having one of the most fragile ecosystems (Feng et al., 2010; Li et al., 2009; Zhang et al., 2016). Soil and water loss in this region have severely hindered conservation of the local ecosystem as well as economic and social development (Zhao et al., 2013). Thus, new approaches to reducing soil and water loss in the region are urgently required.

In recent years, the implementation of several soil and water conservation measures on the Loess Plateau has greatly changed the local land use and vegetation coverage, substantially affecting gully catchments. Previous studies have shown that terracing can influence catchment areas by decreasing the hydrological connectivity among slope surfaces (Zhang et al., 2014a), and that vegetation coverage exceeding 60% in upslope drainage areas could decrease the effective drainage area for controlling gully expansion (Li et al., 2015). However, these studies were primarily based on statistical analyses of regional erosion amounts and the relationship among factors influencing erosion. It thus remains necessary to further analyze the impacts of changes in catchment area on gully erosion through field observations.

The objectives of this study were to present a new framework for studying changes in gully erosion on the Loess Plateau over the past 40 years, and to analyze the influence of changes in catchment area on gully incision by employing high-precision aerial remote sensing observations. This involved: (1) Collection of aerial photographs from 1976 and acquisition of comparable UAV remote sensing observations in 2017 to define gully conditions at two points in time; (2) Estimating changes in gully volume and the erosion modulus; (3) Analyzing the relationship between changes in catchment area and the erosion moduli of gullies.

2. Study area

The Loess Plateau (100°54′–114°33′ E, 33°43′–41°16′ N) is located in the middle reaches of the Yellow River basin in northern China (Zhao et al., 2013). This region stretches over > 600,000 km^2 and is covered by highly erodible loess layers averaging 100 m thick (Fig. 1a). The combined effects of frequent high-intensity storms during summer, a steep landscape, low vegetation cover, and highly erodible soil have made the Loess Plateau one of the most severely eroded areas in the world (Li et al., 2009). In addition, sinkholes (caves formed by underground erosion) are common in the area; their number and volumes also influence gully erosion. Such erosion has had a significant impact

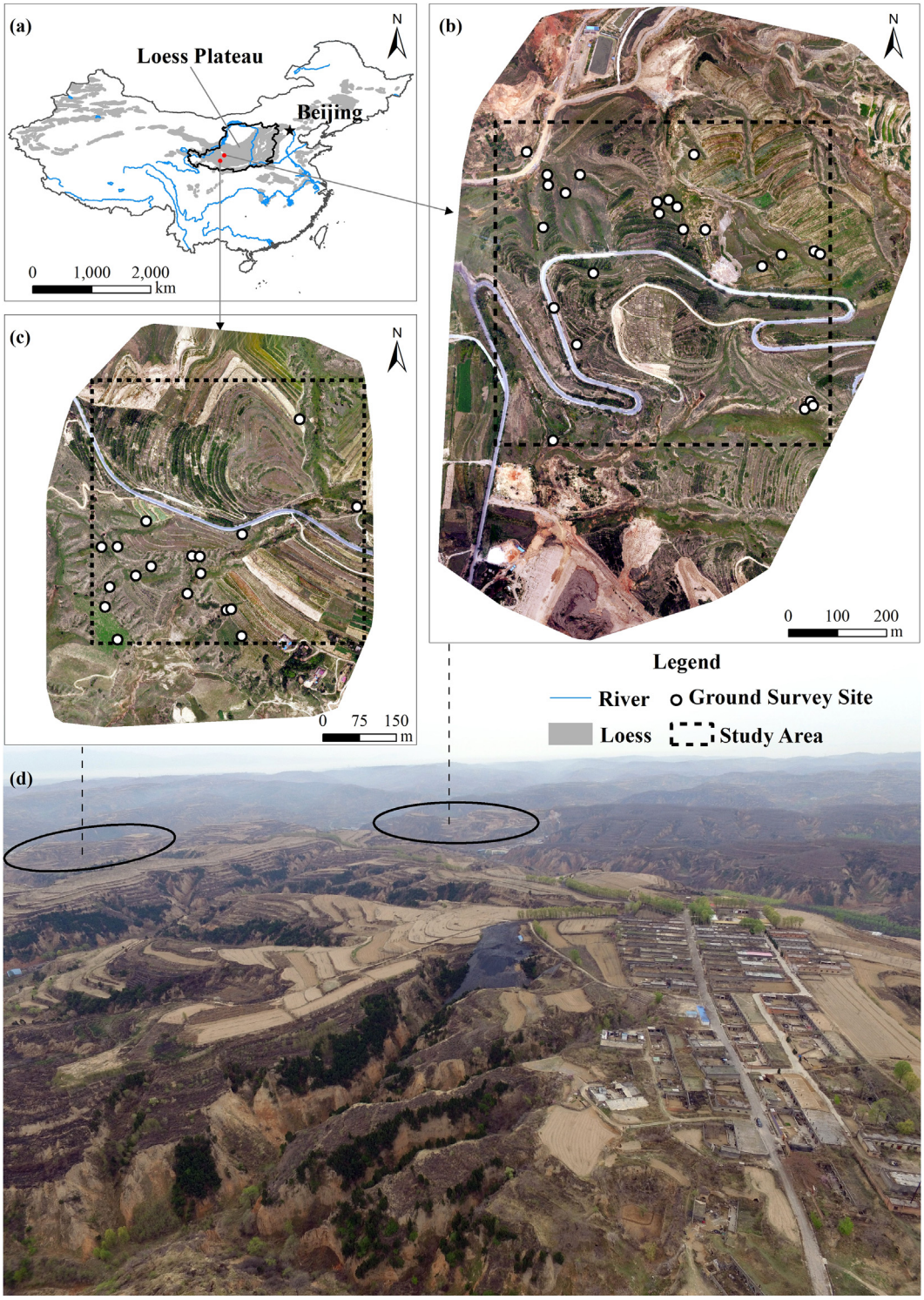

Fig. 1. Location and imagery of the study area: (a) General location and loess distribution within China; (b) Pilot area S1; (c) Pilot area S2; (d) Typical gully erosion landscape on the Loess Plateau. Black boxes indicate locations of the two pilot areas.

on the ecological security of the Yellow River (Sun et al., 2014), produced one of the most fragile ecosystems in the world (Jiang et al., 2016), hindered local conservation efforts, and restricted economic and social development (Zhao et al., 2013). The region urgently needs new approaches to reducing soil and water loss.

The prefecture-level city of Guyuan is representative of the region (Fig. 1), with low rocky mountain and loess hills. The area has a semi-arid climate that is cold and dry in the winter but hot and humid in the summer. The mean annual temperature is 5–8 °C; annual precipitation is ~470 mm (König et al., 2014; Zhen et al., 2009). Precipitation is unevenly distributed within a given year, with > 60% concentrated in July, August, and September. The main regional problems are harsh environmental conditions, land degradation, and low economic development (Zhen et al., 2009; Zhu et al., 1986). As of 2006, population density was 133 person·km^{-2}; out of a population of 1.5 million, 89% were farmers. The average income per rural household was RMB 3477,

nearly half the national average in 2010 (König et al., 2014). In this low-income, high-population-density area experiencing serious land degradation, policymakers and stakeholders are aware of the need to mitigate ecosystem damage, improve agricultural productivity, and farmer income. Although soil and water conservation erosion reduction has been given top priority, this will not succeed until gully development processes are fully understood.

Two pilot areas characterized by abundant loess hills and gullies (S1, Fig. 1b and S2, Fig. 1c) were identified for this study. S1 covers 0.45 km^2 with an elevation range of 1767–1880 m, while S2 covers 0.30 km^2 with an elevation range of 1817–1929 m. Gully erosion is intense in both areas (Fig. 1d), with a mean density of ~3.6 km km^{-2}.

3. Methods and data

Terrestrial imagery from different time periods is needed to explore gully erosion mechanisms. In order to identify changes in gullies and surrounding surface conditions, early gully catchment boundaries and level terrace areas within each catchment were extracted from DOMs (digital orthophoto maps) and DSMs (digital surface models) produced using high-resolution aerial photographs from 1976; the equivalent recent data within each catchment were extracted from high-resolution 2017 UAV-derived DOMs and DSMs. Comparison of the two allowed the determination of gully volume change induced by head retreat, sidewall collapse, and incision. This allowed the calculation of erosion moduli and the determination of reasons for gully catchment area change and their impacts on gully development following three stages (Fig. 2).

3.1. Acquisition and processing of UAV imagery

Aerial imagery acquisition was conducted using a DJI Phantom-3-pro small consumer grade UAV (https://www.dji.com/cn) equipped with an ordinary optical camera capable of acquiring high-resolution true-color terrestrial images. Zhang et al. (2018) found that the terrain measurement accuracy of a DJI Phantom-3-pro UAV controlled by the Pix4Dcapture flight control system within a range of 50–100 m flight height could reach the centimeter level. Therefore, the Pix4Dcapture v. 3.1 flight control system (https://pix4d.com/) was used in this study to plan the UAV's flight path by setting the flight height, flight line, picture overlap, camera angle, picture trigger mode, and flight speed, in order to ensure that the UAV could stably and accurately obtain the terrain data.

UAV flight missions were conducted in August 2017 in the same regions as the early aerial photographs from 1976. The flight heights were 170 m for S1 and 150 m for S2. UAV-derived DOMs, DSMs, and point clouds were then generated for the two pilot areas using Pix4Dmapper v. 4.2 professional image processing software (https://pix4d.com/) with spatial resolutions of 7.10 cm for S1 and 6.29 cm for S2. This software proved highly reliable for such data processing, as shown by previous studies (Zhang et al., 2018; Zhao et al., 2017).

3.2. Acquisition and processing of early aerial photographs

All 211,976 aerial photographs were printed (at a scale of 1:16,000), so the necessary images were converted to 1200 dpi digital files using an Epson Perfection V600 Photo Scanner. Pix4Dmapper automatically processed these digital images based the image hue and texture to derive DOMs, DSMs, and point clouds.

Next, ENVI v. 5.3 software (http://www.harrisgeospatial.com/) was used to select evenly spaced ground control points (i.e., road junctions or farm fields) in both sets of DOMs. The registered DOMs and DSMs were georeferenced using the WGS 1984 datum and UTM projection (zone 48 N) based on a UAV-derived DOM as a reference. Considering the spatial resolution of early aerial photographs cannot reach that of the drone, we resampled both datasets to a pixel size of 0.5 m for subsequent calculations.

3.3. Ground survey methods

A ground survey was conducted at the same time as the UAV observations to measure sinkhole depth and area as well as eight physical parameters related to earthworks from road construction in the study areas. The latter could be accurately measured for validation of remotely sensed volume change by comparing the original ground morphology with the construction-related changes. Where soil was built up

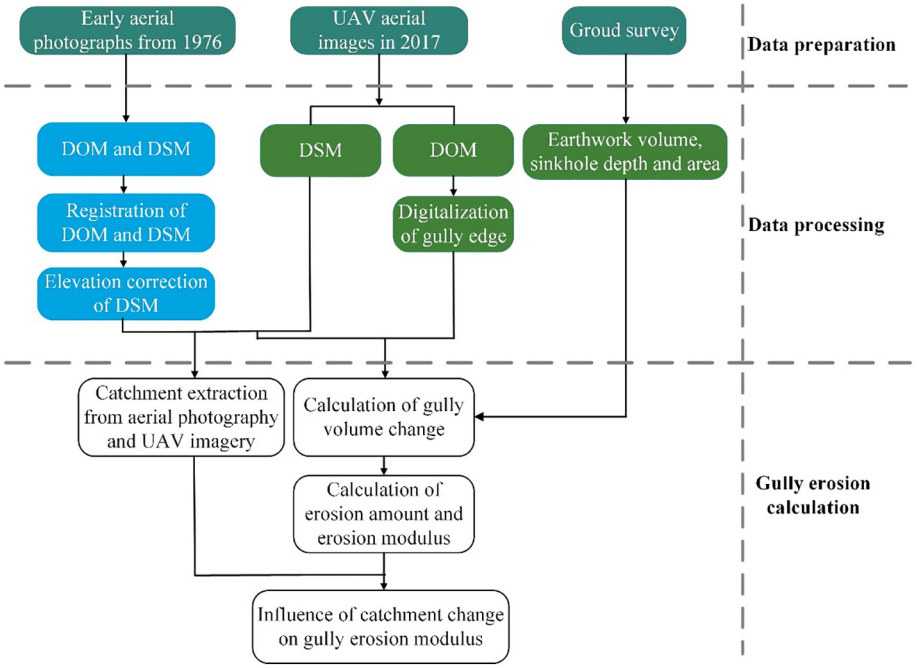

Fig. 2. Flowchart of gully development monitoring based on aerial and remote sensing data. DOM refers to digital orthophoto map, and DSM refers to digital surface model.

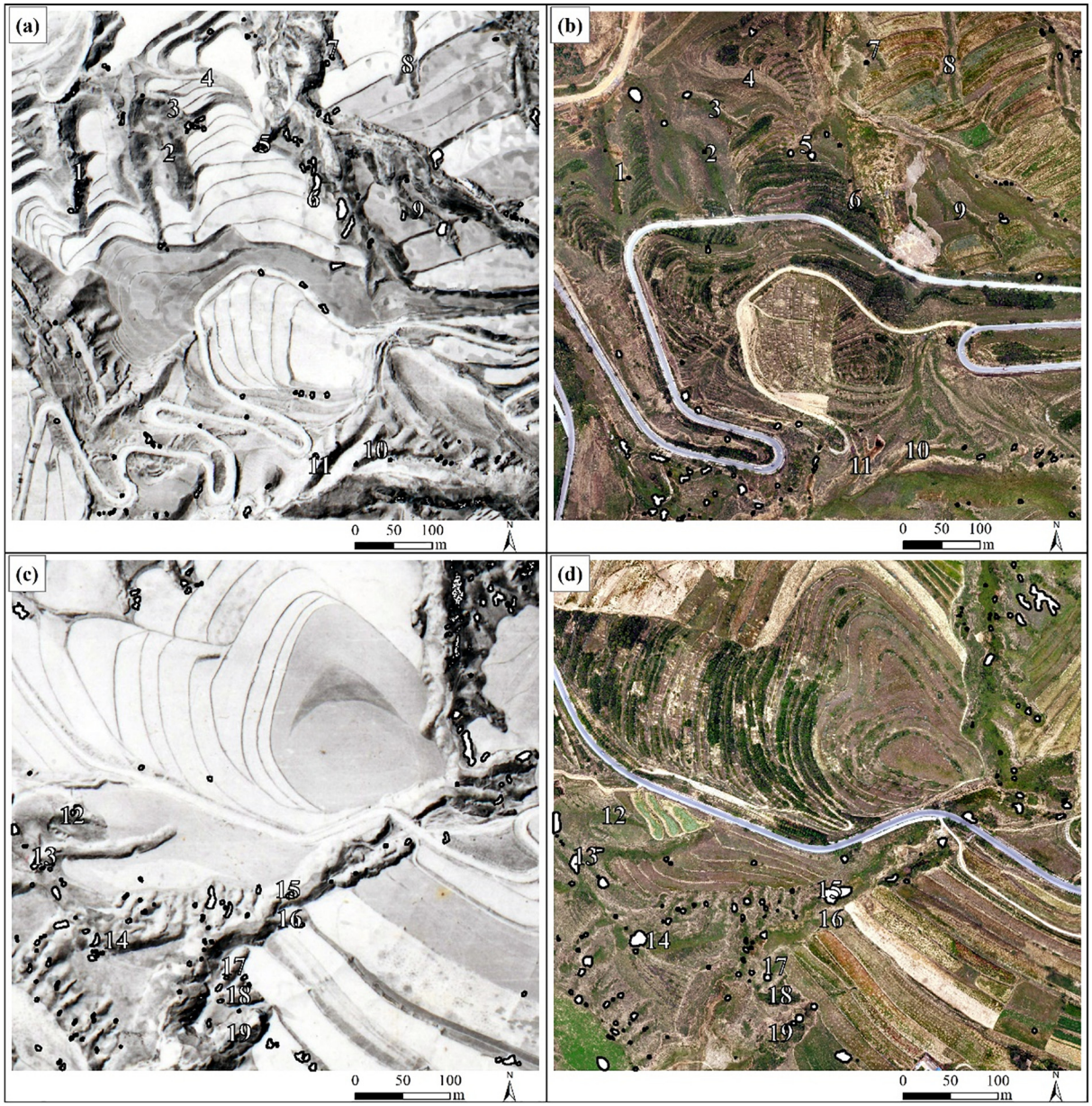

Fig. 3. Registered digital orthophoto maps (DOMs) and distribution of gullies and sinkholes used in this study. (a) DOM derived from 1976 aerial photographs for S1; (b) 2017 UAV-derived DOM for S1; (c) DOM derived from 1976 aerial photographs for S2; (d) 2017 UAV-derived DOM for S2. Numbers indicate locations of gullies listed in Table 1. Polygons with black outline and white fill color indicate locations of sinkholes.

by construction (an accumulation body), these parameters included side slope angle of each cross-section, side slope length of each cross-section, top width of each cross-section, and distance between adjacent cross-sections. Where soil was excavated, these included road width of each cross-section, roadside slope angle of each cross-section, roadside slope length of each cross-section, and distance between adjacent cross-sections. The average end area (AEA) method (Epps and Corey, 1990; Slattery et al., 2012) was used to calculate earthwork volumes of accumulation bodies and excavations using these eight parameters. The depth and area of randomly selected sinkholes, a characteristic feature of loess regions (Zhou and Shen, 2013), were determined using a tape measure in order to establish the relationship between depth and area; based on this, the depth of any sinkhole could be calculated using the UAV-determined sinkhole area.

The ground survey measured parameters for 35 sinkholes, one accumulation body, and one road excavation from August 20–27, 2017. For the accumulation body and road excavation, multiple cross-sections were first set at a certain distance, then irregular cross-sections were divided into simple geometric shapes such as rectangles, trapezoids, or triangles. Second, the relevant edge length and angle parameters of these simple geometric shapes were measured to calculate their area and the cross-sectional area was calculated by summing the areas of the geometric shapes. Finally, the earthwork volume between adjacent cross-sections was calculated by the mean area of the adjacent cross-sections multiplied by the distance of the adjacent cross-sections. The total earthwork volume was calculated by summing the earthwork volumes among all adjacent cross-sections (Epps and Corey, 1990; Slattery et al., 2012).

3.4. Calculation of gully volume change, erosion amount, and erosion modulus

Gully volume change, erosion amount, and erosion modulus are important indicators of gully development; these were calculated based

on the differences between UAV-derived DSMs and elevation-corrected DSMs derived from early aerial photographs (Marzolff and Poesen, 2009). To achieve this, a new method was developed based on the research of Martínez-Casasnovas (2003):

$$EM_{gully} = Erosion_{gully}/(Area \times year), \quad (1)$$

$$Erosion_{gully} = Soil_{\text{bulk density}} \times (\Delta Volume_{\text{gully}} + Volume_{\text{Sinkhole}}), \quad (2)$$

$$\Delta Volume_{\text{gully}} = \sum_{i=1}^{n} (DSM_{\text{UAV}} - DSM_{\text{Aerial photo}}) \times L^2, \quad (3)$$

where EM_{gully} is the erosion modulus in t km^{-2} a^{-1}, *Area* is the gully catchment area in km^2, *year* is the study period, $Erosion_{gully}$ is the total soil loss induced by gully erosion and sinkhole development in t, $Soil_{\text{bulk density}}$ is the soil bulk density (1.4 t m^{-3} in the study area) (Hou et al., 2012; Zhang et al., 2014b; Zhang et al., 2015), $Volume_{\text{Sinkhole}}$ is the total volume of sinkholes developed nearby the gully in m^3, $\Delta Volume_{\text{gully}}$ is the gully volume change in m^3, DSM_{UAV} and $DSM_{\text{Aerial photo}}$ are the elevations of UAV images and early aerial photographs in the same pixel within the digitized gully edge in m, L is the raster resolution of the DSM in m, and n is the count of pixels within the digitized gully edge.

4. Results

4.1. Gully erosion sources

Gully erosion in this study came from two sources: the gullies themselves and nearby sinkholes.

4.1.1. Gully identification

Using a UAV-derived DOM as a reference, image registration was conducted for the DOMs and DSMs derived from early aerial photographs in 1976. The image registration root mean-squared errors (RMSEs) were 0.96 pixels for S1 and 0.59 pixels for S2. The registered DOMs at the two pilot areas are shown in Fig. 3. A total of 19 gullies with complete catchments were digitized by visual interpretation based on the UAV-derived DOMs (Fig. 3; Table 1).

4.1.2. Sinkhole development

Based on visual interpretation from DOMs and field surveys, 87 sinkholes were digitized for S1 in 1976 and 101 in 2017, while S2 contained 120 in 1976 and 126 in 2017 (Fig. 3).

A statistical relationship between the measured areas and depths of 35 sinkholes (20 sinkholes in S1 and 15 in S2) in 2017 (Table 2) was obtained by determining the line of best fit, with a correlation coefficient $R^2 = 0.92$ demonstrating a positive correlation between sinkhole area and depth (Fig. 4). Using this relationship, the depth of all sinkholes in both 1976 and 2017 was calculated using the areas retrieved from the early aerial photographs and UAV imagery; volume was then calculated by multiplying depth by area. Sinkhole volumes in S1 varied from 18.35 m^3 (mean, 1976) and 1596.46 m^3 (total volume, 1976) to 13.97 m^3 (mean, 2017) and 1411.29 m^3 (total volume, 2017). Sinkhole volumes in S2 changed from 12.76 m^3 (mean, 1976) and 1531.39 m^3 (total volume, 1976) to 14.37 m^3 (mean, 2017) and 1810.49 m^3 (total volume, 2017).

4.2. Gully volume change with elevation correction

4.2.1. DSM elevation correction

Systematic errors existed between the registered DSMs derived from 1976 aerial photographs and the UAV-derived DSMs generated by Pix4Dmapper. Elevation correction of the former was conducted by selecting points on stable areas (i.e., roads and flat cultivated land); 76 correction points were selected for S1 and 39 for S2 and the linear fit of elevations derived from aerial photographs and UAV images was obtained (Fig. 5). The final corrected DSMs were obtained by applying the elevation-fitting expressions to the corresponding registered DSMs in 1976 (Fig. 6). The corrected elevation varied from 1764 to 1893 m in S1 and 1811–1942 m in S2.

4.2.2. Gully volume change

Elevation changes in S1 and S2 from 1976 to 2017 were computed by subtracting the values in the earlier DSM from those in the later UAV-derived DSM, such that negative changes indicate erosion and positive changes indicate deposition (Fig. 7). Elevation changes exhibited high spatial variability, varying from −19 to 43 m in S1 and −27 to 19 m in S2. In S1, erosion was mainly distributed in the central and northern areas, while deposition mainly occurred in the south. In S2, erosion was mainly distributed in the northeastern and northwestern areas, while deposition mainly occurred in the central and southern areas. Gully volume change was computed using Eq. (3) (Table 1), ranging from 133.70 to 8923.53 m^3 with a mean value of 1621.89 m^3.

4.2.3. Validation of volume change

Volume changes were validated by field surveys in S1 (Fig. 8), where the changes in regions A, B, and C were caused by human interference. Region A displayed high accumulation caused by construction debris, region B experienced both excavation and accumulation driven by road construction, and region C experienced engineering excavation. Regions D and E were mainly naturally eroded, with the most severe erosion in gully interiors, mainly caused by incision and head retreat. Volume change in S1 was calculated using Eq. (3) with aerial remote sensing data. The volume change in regions A and B of S1 were ground-measured and calculated using the AEA method to validate volume change using Eq. (3). The relative error of the volume changes calculated with Eq. (3) from aerial remote sensing data were both < 10% compared with the measured volume change (Table 3), demonstrating the high-quality performance of our method.

Table 1
Gully area and volume changes at pilot areas S1 and S2.

Pilot area	Gully number	Gully area (m^2)	Eroded volume (m^3)	Pilot area	Gully number	Gully area (m^2)	Eroded volume (m^3)
S1	1	2279.59	2365.09	S2	12	786.72	562.29
	2	5004.10	8923.53		13	274.01	725.72
	3	1551.38	519.17		14	1247.78	1278.95
	4	2614.70	1303.16		15	542.94	1217.67
	5	997.89	951.05		16	621.83	139.60
	6	468.02	534.43		17	672.78	133.70
	7	642.96	266.97		18	962.34	387.10
	8	1667.00	1086.95		19	2653.60	2168.82
	9	2164.91	3691.60		–	–	–
	10	755.85	1732.55		–	–	–
	11	1590.54	2827.52		–	–	–

Table 2
Measured areas and depths of sinkholes.

Pilot area	No.	Area (m^2)	Depth (m)	Pilot area	No.	Area (m^2)	Depth (m)
S1	1	74.38	2.73	S2	21	16.14	1.17
	2	63.49	2.59		22	88.18	3.24
	3	228.39	5.89		23	82.66	3.06
	4	7.92	0.72		24	45.51	1.95
	5	1.06	0.17		25	118.87	3.82
	6	40.93	2.88		26	16.66	1.14
	7	34.61	1.30		27	215.79	7.39
	8	10.80	0.90		28	25.67	0.81
	9	7.17	0.41		29	34.63	1.14
	10	13.09	1.14		30	36.63	1.04
	11	6.04	0.50		31	19.93	0.89
	12	31.47	1.57		32	31.15	1.47
	13	12.05	1.31		33	141.75	4.13
	14	10.92	0.56		34	37.51	2.23
	15	25.92	1.40		35	43.95	2.61
	16	9.85	0.74		–	–	–
	17	2.68	0.50		–	–	–
	18	51.25	1.85		–	–	–
	19	13.99	0.88		–	–	–
	20	2.85	0.76		–	–	–

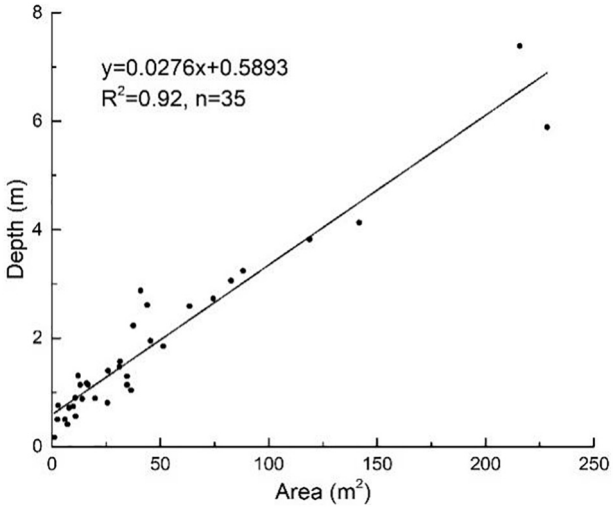

Fig. 4. Scatter plot and relationship between sinkhole area (m^2) and depth (m).

4.3. Gully erosion

4.3.1. Erosion amount and erosion modulus

The gully catchment areas in 1976 were extracted by Hydrology tools in ArcGIS v. 10.3 (https://www.esri.com/). The total volume of sinkholes within each gully catchment varied from 0 to 87.71 m^3. The gully erosion amount and erosion modulus were computed by Eqs. (1) and (2) (Table 4). The gully erosion amount varied from 187.17 to 12,513.81 t, with a mean value of 2283.05 t. The minimum value of the erosion modulus was 1686.57 $t\,km^{-2}\,a^{-1}$, the maximum was 7391.68 $t\,km^{-2}\,a^{-1}$, and the mean value was 4364.69 $t\,km^{-2}\,a^{-1}$.

4.3.2. Erosion modulus reliability analysis

We conducted a comparison of erosion moduli between this and other studies (Li et al., 2006; Li et al., 2003b; Pang et al., 2013; Quan et al., 2011) in similar regions due to the lack of measured erosion moduli in our study area (Table 5). The erosion moduli in our study varied from 1686.57 to 7391.68 $t\,km^{-2}\,a^{-1}$, similar to those in previous studies, which ranged from 2901.00 to 8000.00 $t\,km^{-2}\,a^{-1}$. Our average erosion modulus (4364.69 $t\,km^{-2}\,a^{-1}$) also fell within the range of previous results. This comparison indicates that the erosion moduli we calculated from aerial remote sensing data were reliable.

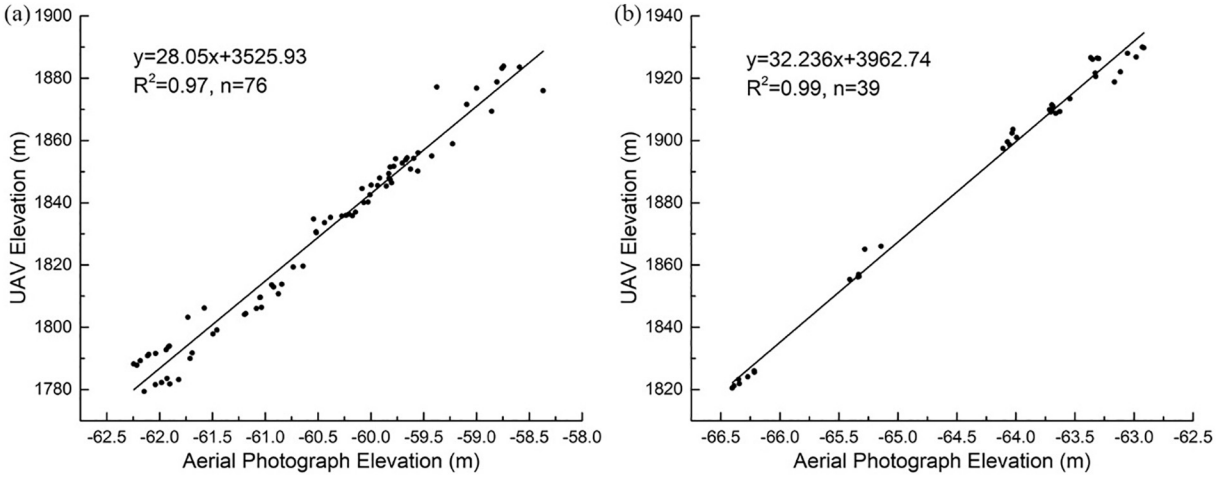

Fig. 5. Scatter plot and relationship between Pix4Dmapper-derived original aerial photograph elevation and UAV elevation (m) for (a) S1 and (b) S2. Negative elevation values of X axis were caused by the lack of image geolocation of early aerial photographs. These original negative DSM elevation values were relative values, and had no effect on the results of this study.

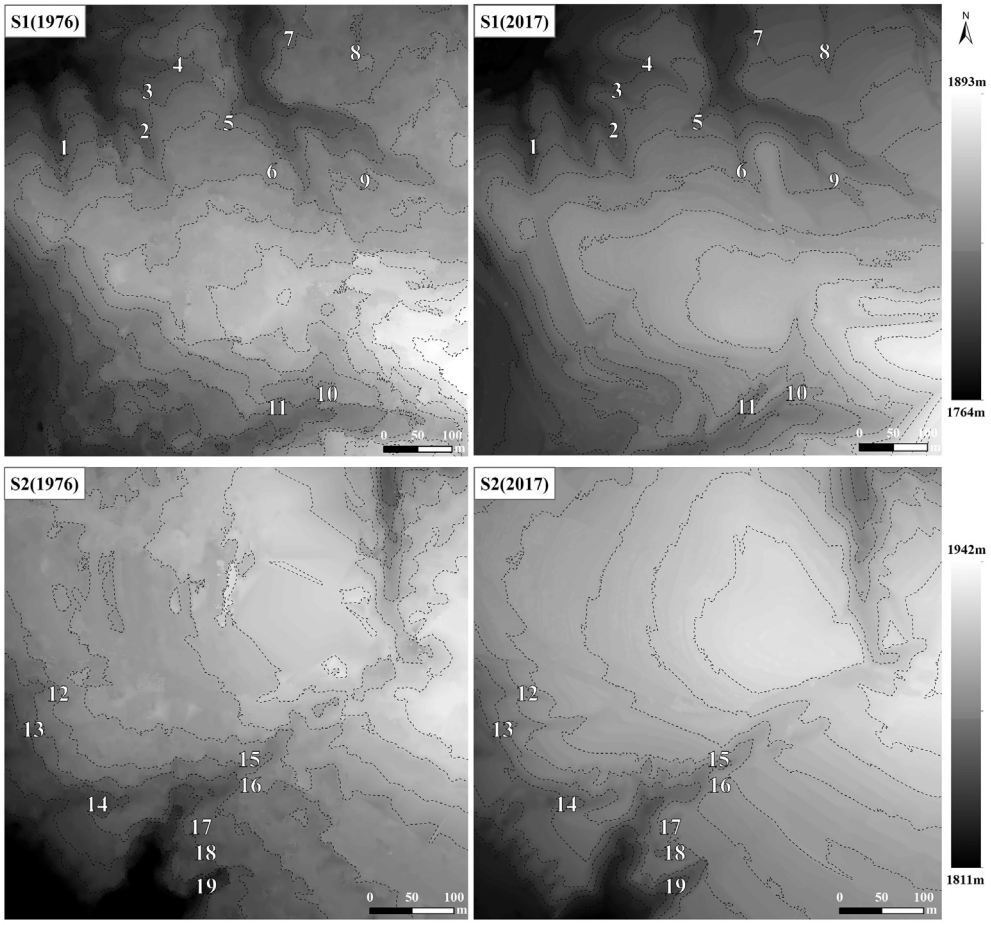

Fig. 6. Corrected digital surface models and UAV-derived digital surface models (DSMs).

5. Discussion

5.1. Sinkhole development on the Loess Plateau

Soil pipe or sinkhole is a subsurface process that usually consists of inlet, path and outlet. Sinkhole detection is very difficult due to its subsurface nature. High-resolution aerial photographs are often used to detect the spatial distribution of sinkhole inlet, but do not allow the identification of complete underground sinkhole path network. This may underestimate the sinkhole-affected area by 50% (Bernatek-Jakiel and Poesen, 2018). Zhu (2003) studied the development process of loess sinkholes on the Loess Plateau by field measurements, and found majority of sinkhole erosion was produced by the initiation and enlargement of sinkhole inlets rather than sinkhole paths (volumetric

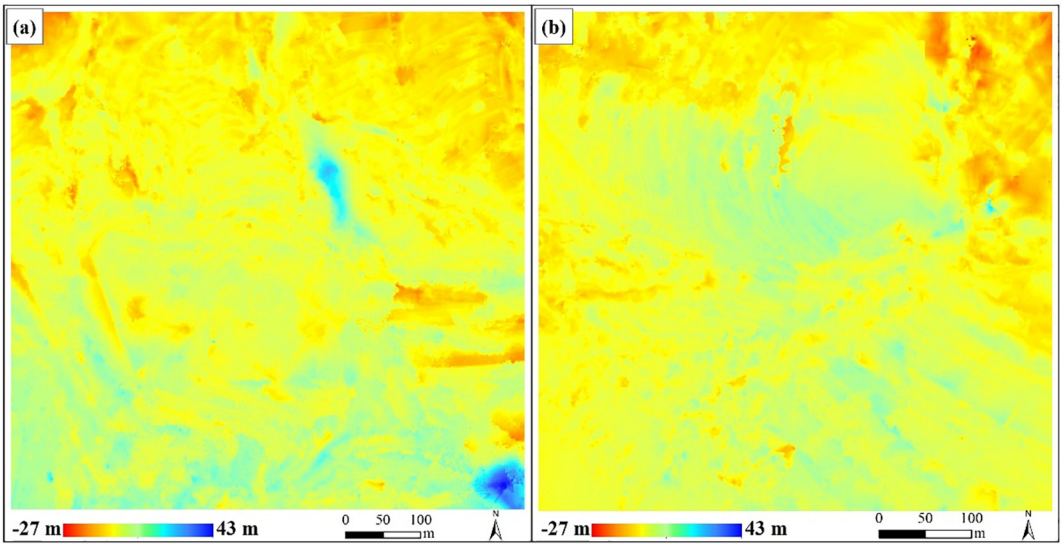

Fig. 7. Elevation changes from 1976 to 2017 in (a) S1 and (b) S2.

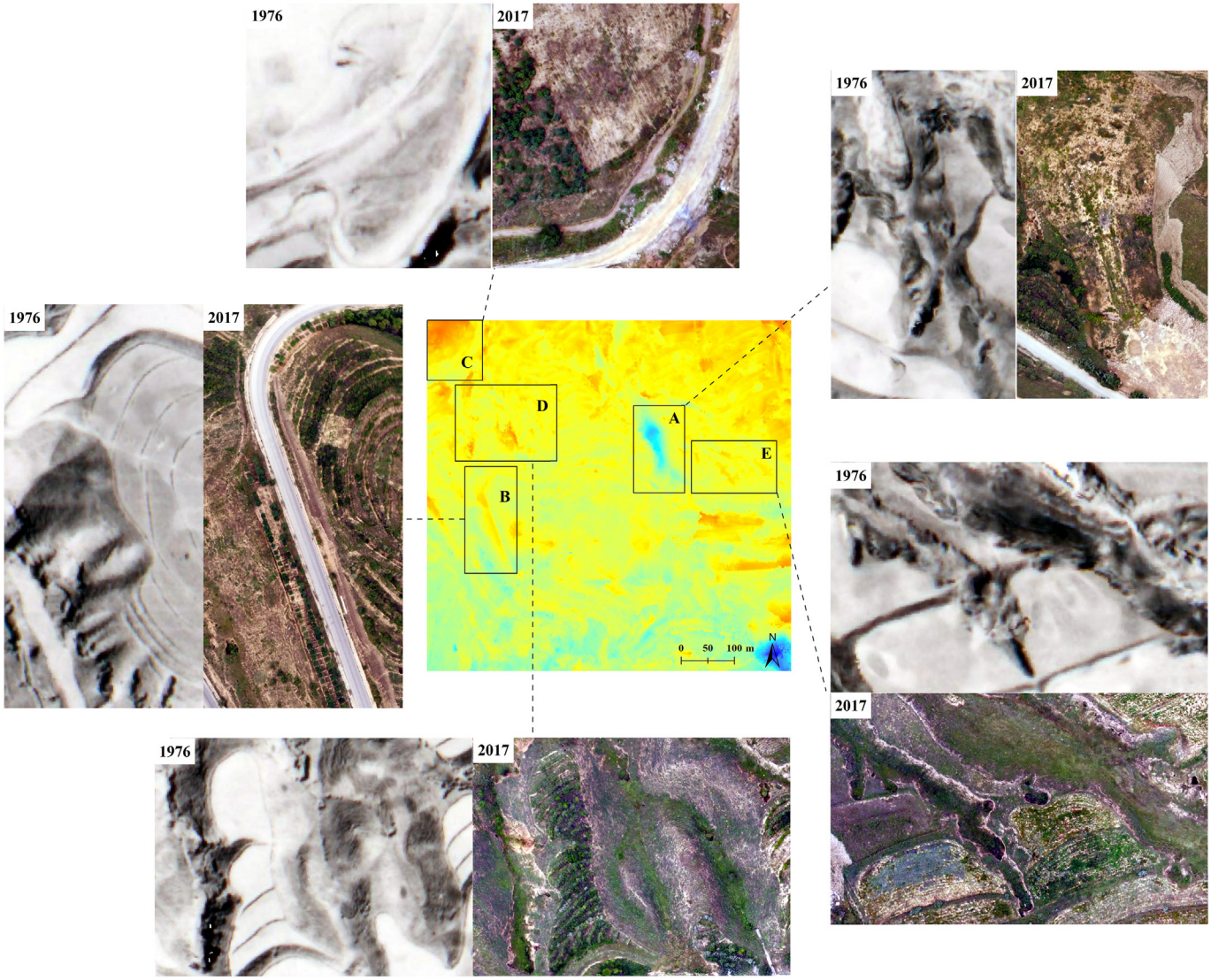

Fig. 8. DSM changes in S1 (center) with five black boxes indicating typical regions A, B, C, D, and E. Photo pairs (surrounding) compare 1976 aerial photos and 2017 UAV aerial images in these regions.

Table 3
Validation of volume changes calculated from aerial remote sensing data.

Pilot area	Region	Measured Volume (m^3)	Estimated change (m^3)	Relative error
S1	A	79,516.65	73,505.64	−7.56%
	B	7378.42	6717.04	−8.96%

ratio of 40.8: 1 between inlets and paths). This demonstrated it is feasible to estimate the erosion volume caused by sinkhole on the Loess Plateau using the surface method of high-resolution aerial imagery due to the great disparity in volumes between inlets and paths.

Due to the differences in the conditions of formation of sinkholes, the size and intensity of sinkholes in different regions were quite different. Our observations showed that the average diameter of sinkholes in S1 and S2 regions in 2017 were separately 4.87 m and 4.71 m, which were much larger than the average diameter of 1.1 m on the loess-derived soils in central Belgium (Verachtert et al., 2010). The mean density of sinkholes of our study area was 3.03/ha (2.24/ha in S1 and 4.2/ha in S2), which was 3.12 times that of Golestan Province, Iran (Hosseinalizadeh et al., 2018). According to the classification criteria of sinkhole development intensity on the Loess Plateau proposed by Peng et al. (2018), pilots S1 and S2 both belonged to the strong developed zone. In addition, sinkhole volumes were calculated based on aerial images in our study. The results indicated that the mean volumetric intensity of sinkholes in our study area was 4295.70 $m^3 km^{-2}$ (3136.2 $m^3 km^{-2}$ in S1 and 6034.96 $m^3 km^{-2}$ in S2), which is lower than 224,277 $m^3 km^{-2}$ of Yangdaogou on the Loess Plateau (Zhu, 2003), but higher than 260.3 $m^3 km^{-2}$ in Maesnant, England (Jones, 1997). The above comparisons indicated that loess sinkhole in Guyuan region on the Loess Plateau represented some of the largest in non-karst regions in the world (Zhu, 2003).

Gully erosion has been frequently observed to be associated with sinkhole development in many parts of the world. Sinkholes usually occur in special topographic locations, and the formation process of sinkholes in different locations is also different (Peng et al., 2007; Peng et al., 2018). In our study, sinkholes were mainly distributed at the gully edges, gully walls and gully bottoms. In S1 and S2 regions, the number of sinkholes located within a distance of 50 m from the gully drainage network separately accounted for 65.35% and 95.23% of all the sinkholes, which were higher than 61.38% of Golestan Province, Iran (Hosseinalizadeh et al., 2018). In S1 and S2 regions, the sinkholes located inside the gullies accounted for 50.50% and 66.67% of all the sinkholes in 2017, respectively. Liu et al. (2015) also found gully was

Table 4
The erosion amounts and moduli of the studied gullies.

Pilot area	Gully number	$Volume_{sinkhole}$ (m^3)	Erosion amount (t)[a]	Erosion moduli ($t\,km^{-2}\,a^{-1}$)
S1	1	–[b]	3311.13	3958.22
	2	14.9	12,513.81	7391.68
	3	–	726.83	3831.08
	4	–	1824.42	5466.26
	5	–	1331.47	3162.93
	6	–	748.20	4035.59
	7	–	373.76	3202.18
	8	–	1521.73	2913.86
	9	3.27	5172.82	7046.28
	10	5.65	2433.48	6057.65
	11	17.02	3982.36	6636.82
S2	12	–	787.20	3664.82
	13	11.14	1031.60	3541.12
	14	28.73	1830.75	4808.66
	15	87.71	1827.54	3162.93
	16	–	195.44	1686.57
	17	–	187.17	2972.89
	18	–	541.94	2615.05
	19	–	3036.34	6774.53

[a] Erosion amount means the total soil loss induced by gully erosion and sinkhole developed nearby the gully edge in t.

[b] '–' symbol indicates there are no sinkholes within the region between gully edge boundary and its watershed boundary.

the main area for the formation and development of loess sinkhole. These sinkholes located inside gullies on the Loess Plateau were mainly caused by the effect of shootpool action of falling surface water on the loess materials of lower part. In particular, due to the falling surface water of the gully head, beads-shaped sinkholes are often formed in the gully bed, which may lead to the progress of gully head and the overall deepening of gully bed (Zhu, 2012).

Our monitoring results also showed that sinkholes outside the gullies were rarely found on terraces, which was consistent with the survey results of Zhu (2003) in Yangdaogou watershed on the Loess Plateau. However, Romero Díaz et al. (2007) observed piping process in abandoned agricultural terraces in southeast Spain and concluded terrace in dispersive materials actually enhanced piping. The dispersive materials in their region was mainly composed of calcium carbonate and clay, with the chemical soil properties of high exchangeable sodium percentage which favours soil clay dispersion, and initiation of the piping process at subsurface levels. Loess on the Loess Plateau, with low clay content, high silt content, low-sodium content, loose and porous, collapsibility when exposed to water, and developed vertical joints, was different from the characteristics of dispersive materials in southeastern Spain (Faulkner, 2006; Zhu, 2003). The main cause of this kind of sinkholes located outside gullies on the Loess Plateau is that runoff with large contributing drainage area concentrate and infiltrate intensely in the location with negative topography (Faulkner, 2006; Li et al., 2003a; Peng et al., 2018; Wang, 1989; Zhu, 2003). Terracing on hillslopes of the Loess Plateau has been proved to be an effective measure to reduce the occurrence of sinkholes (Zhu, 2003). Due to the construction of level terraces, the slope of the surface is significantly reduced, and the runoff of the hillslope is intercepted, resulting in a significant decrease in the catchment area. The amount of water received by terraces usually comes only from the precipitation received by its bench surface. Therefore, there is no intensely concentrated infiltration on the flat bench surface to form a sinkhole.

5.2. Gully catchment area change from 1976 to 2017

Gully catchment area varied from 1574 to 42,324 m^2 in 1976 and from 758 to 40,669 m^2 in 2017 (Fig. 9, Table 6), but all areas decreased from 1976 to 2017 at various scales. Gullies 2, 4, 9, 10, and 19 were relatively stable (< 5% change) while the remaining 14 areas shrunk by −19.56% to −77.88%. The 1976 landscape consisted of mostly cultivated, sloped lands that had been converted to level terraces by 2017, resulting in reduced gully catchment areas by intercepting upslope runoff and reducing hydrological connectivity within the slope (Arnáez et al., 2015; Shi et al., 2012).

5.3. Effect of decreased catchment areas on erosion moduli

A power function relationship was obtained by scatter plot fitting between the gully catchment areas in 2017 and the corresponding erosion moduli (Fig. 10), showing a positive correlation. Other studies have also showed that there existed a positive power function relationship between catchment area and gully erosion rates, and the larger the catchment area is, the more severe the gully erosion is (Marzolff et al., 2011; Vandekerckhove et al., 2003; Vandekerckhove et al., 2001; Vandekerckhove et al., 2000).

Plotting the changes in gully catchment area against the erosion moduli showed that larger decreases in catchment area were correlated with smaller gully erosion moduli (Fig. 11). These results indicate that decreases in catchment area correspond with less runoff into the gully, resulting in a weakening of the scouring effect and a correspondingly smaller erosion modulus. Since the two pilots S1 and S2 had small spatial extent and were spatially adjacent, the effects of spatial variability of lithology, soil and climate on gully development could be negligible. Therefore, the change in catchment areas between 1976 and 2017 was a dominant factor in the erosion modulus change.

5.4. Effect of terrace construction on catchment area

The effects of level terraces on gully erosion can be divided into two aspects, the primary reduction in sediment production and the secondary reduction of sediment via interception from upslope (Liu et al., 2014; Luo et al., 2015). In order to separate the influence of the constructed terraces themselves on gully erosion moduli, the five gullies that exhibited little change in their catchment areas were chosen (2, 4, 9, 10, and 19); their erosion moduli had no significant correlation with the change% in level-terraced areas within the catchment area from 1976 to 2017 ($R^2 = 0.09$). Field investigations showed that the quality of terraces in 1976 and 2017 above the selected 5 gullies were effectively the same, and there was no fundamental change in the runoff and sediment interception effect by the terraced fields, so the catchment area has remained nearly constant.

The growth rates of level, terraced areas in 2017 relative to 1976 were calculated for the remaining 14 gullies and plotted against gully erosion moduli (Fig. 12), showing that an increase in the level, terraced area enhanced the interception of runoff and sediment transport from

Table 5
Comparison between calculated erosion moduli and results of previous studies.

Reference	Location	Period	Erosion modulus/range ($t\,km^{-2}\,a^{-1}$)	Erosion type
Quan et al. (2011)	Liupan Mountain Region, southern Ningxia	1986–2000	5000.00–8000.00	Water erosion
Li et al. (2003b)	Yangjuangou catchment, near Yan'an city, northern Shaanxi province	1992–1996	6273.00	Water erosion
Li et al. (2006)	Zhifanggou watershed, Ansai County, Shaanxi Province	1991–1995	2901.00	Water erosion
Pang et al. (2013)	Zhifanggou watershed, Ansai county, Shaanxi Province	1985–2010	3153.54	Water Erosion
This paper	Guyuan, southern Ningxia	1976–2017	4364.69	Water Erosion

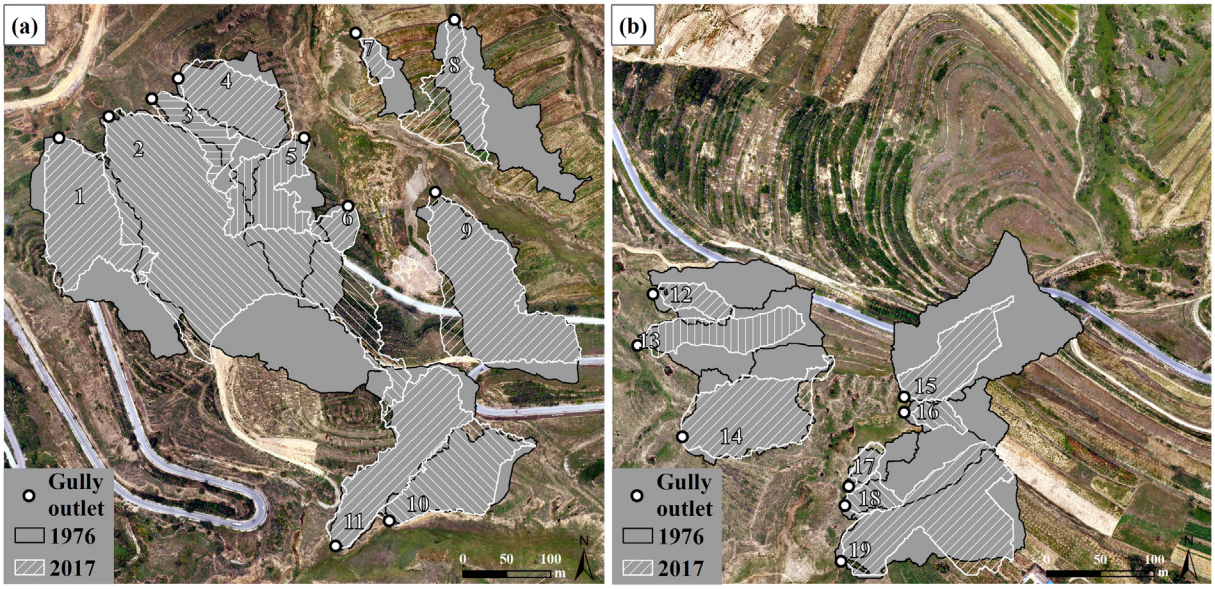

Fig. 9. Comparison of gully catchments in 1976 and 2017 in (a) S1 (a) and (b) S2.

Table 6
Changes in gully catchment areas.

Pilot area	Gully number	Catchment area in 1976 (m^2)	Catchment area in 2017 (m^2)	Area change (%)
S1	1	20,913	12,482	−40.31
	2	42,324	40,669	−3.91
	3	4743	3387	−28.59
	4	8344	8285	−0.71
	5	10,524	7145	−32.11
	6	4635	1859	−59.89
	7	2918	1114	−61.82
	8	13,056	7344	−43.75
	9	18,353	17,848	−2.75
	10	10,043	9941	−1.02
	11	15,001	12,067	−19.56
S2	12	5370	1496	−72.14
	13	7283	3953	−45.72
	14	9518	7551	−20.67
	15	14,445	4179	−71.07
	16	2897	945	−67.38
	17	1574	758	−51.84
	18	5181	1146	−77.88
	19	11,205	10,890	−2.81

upslope, reduced the hydrological connectivity among the slopes, and led to the changes observed in the gully catchment area, thus reducing the erosion modulus.

6. Conclusions

Volume change and erosion moduli are important quantitative indicators of gully erosion. This study monitored the development of gully erosion on the Loess Plateau of China from 1976 to 2017. Changes in gully volumes and erosion moduli were calculated based on registered and corrected DSMs derived from 1976 aerial photographs and 2017 UAV images, and the influence of gully catchment area change on gully erosion was analyzed. Validation of the results suggests that these methods can compensate for the lack of monitoring data for long-term gully development by combining historical aerial photographs and modern UAV remote-sensing observations in the corresponding areas. These methods are also effective for monitoring changes in topography and geomorphology.

Over the study period, the volume change of 19 selected gullies

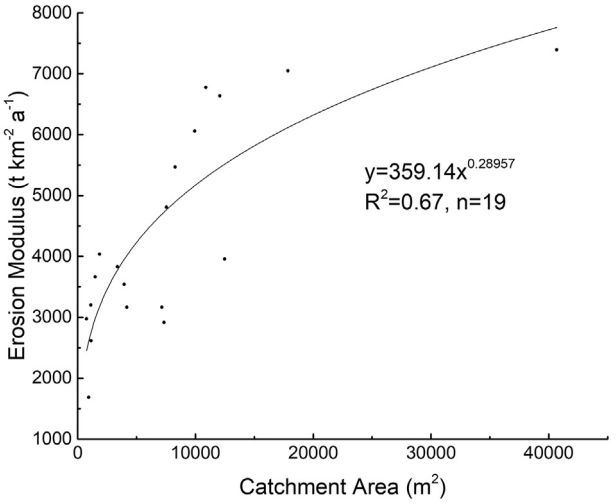

Fig. 10. Scatter plot of gully catchment areas in 2017 and the corresponding erosion moduli.

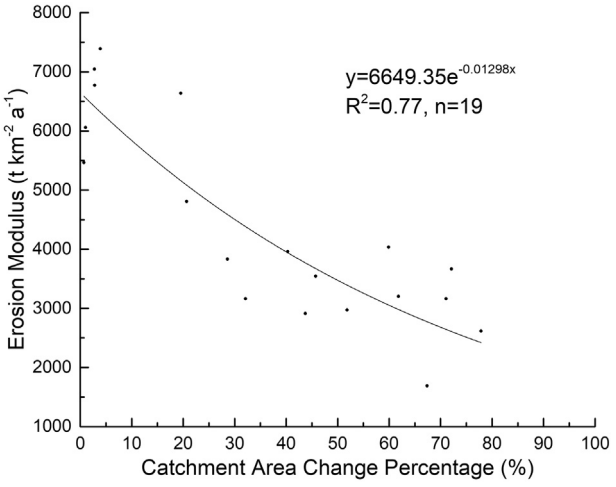

Fig. 11. Scatter plot of gully catchment area change% and corresponding erosion modulus.

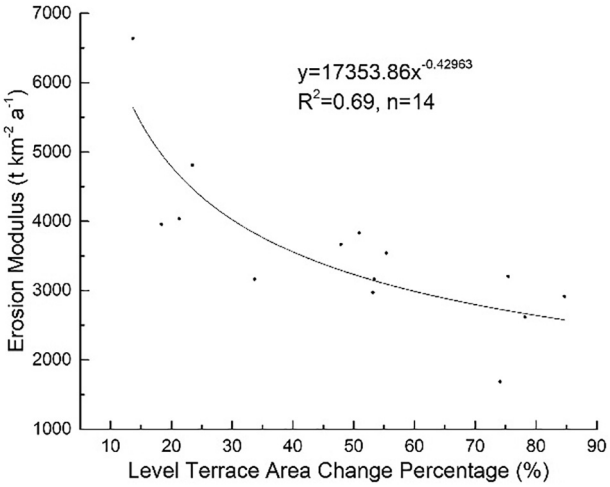

Fig. 12. Relationship between change% of level, terraced areas and erosion moduli when gully catchment area changes substantially.

ranged from 133.70 to 8938.44 m^3 with an average erosion modulus of 4364.69 $t\,km^{-2}\,a^{-1}$. Compared with 1976, the decreases in gully catchment areas by 2017 ranged from 0.71 to 77.88%. This decrease in catchment area is the main reason for changes in the gully erosion moduli. The larger the decrease in catchment area, the smaller the gully erosion modulus is, with an exponential correlation. Thus, reducing gully catchment area can effectively control gully development.

Further, by comparing changes in the underlying ground surface over time, this study showed that an increase in terraced areas in the study area was the main reason for the decrease in the gully catchment area. Terrace construction, especially the conversion of sloped, arable land into level terraces, has enhanced the interception of runoff from upslope, changed the area of the original gully catchment, reduced runoff into the gully, and thus reduced the intensity of gully erosion. These findings indicate that the proper management and maintenance of terraced lands may prevent any weakening in their ability to intercept runoff and sediment from upslope catchment area and thus mitigate or control further gully development.

Acknowledgments

We are grateful to all the reviewers and editors for their valuable comments and efforts on this paper. This study was supported by the National Key Project for R&D (Grant No. 2016YFC0402403), and the National Natural Science Foundation of China (Grant Nos. U1812401 and U1603241), the 111 Project (Grant No. B18006).

Declaration of interest

The authors declare no conflict of interest.

References

Amit, R., Enzel, Y., Mushkin, A., Gillespie, A., Batbaatar, J., Crouvi, O., Vandenberghe, J., An, Z., 2013. Linking coarse silt production in Asian sand deserts and Quaternary accretion of the Chinese Loess Plateau. Geology 42 (1), 23–26.

Arnáez, J., Lana-Renault, N., Lasanta, T., Ruiz-Flaño, P., Castroviejo, J., 2015. Effects of farming terraces on hydrological and geomorphological processes. A review. Catena 128, 122–134.

Bernatek-Jakiel, A., Poesen, J., 2018. Subsurface erosion by soil piping: significance and research needs. Earth-Sci. Rev. 185 (1), 1107–1128.

Cheng, H., Zou, X., Wu, Y., Zhang, C., Zheng, Q., Jiang, Z., 2007. Morphology parameters of ephemeral gully in characteristics hillslopes on the Loess Plateau of China. Soil Tillage Res. 94 (1), 4–14.

d'Oleire-Oltmanns, S., Marzolff, I., Peter, K., Ries, J., 2012. Unmanned aerial vehicle (UAV) for monitoring soil erosion in Morocco. Remote Sens. 4 (12), 3390–3416.

Eltner, A., Baumgart, P., Maas, H.-G., Faust, D., 2015. Multi-temporal UAV data for automatic measurement of rill and interrill erosion on loess soil. ESPL 40 (6), 741–755.

Epps, J.W., Corey, M.W., 1990. Cut and fill calculations by modified average-end-area method. J. Transp. Eng. 116 (5), 683–689.

Faulkner, H., 2006. Piping hazard on collapsible and dispersive soils in Europe. In: Soil erosion in Europe, pp. 537–562.

Feng, X., Wang, Y., Chen, L., Fu, B., Bai, G., 2010. Modeling soil erosion and its response to land-use change in hilly catchments of the Chinese Loess Plateau. Geomo 118 (3–4), 239–248.

Frankl, A., Poesen, J., Deckers, J., Haile, M., Nyssen, J., 2012. Gully head retreat rates in the semi-arid highlands of Northern Ethiopia. Geomo 173-174, 185–195.

Fu, B.J., Meng, Q.H., Qiu, Y., Zhao, W.W., Zhang, Q.J., Davidson, D.A., 2004. Effects of land use on soil erosion and nitrogen loss in the hilly area of the Loess Plateau, China. Land Degrad. Dev. 15 (1), 87–96.

Glendell, M., McShane, G., Farrow, L., James, M.R., Quinton, J., Anderson, K., Evans, M., Benaud, P., Rawlins, B., Morgan, D., Jones, L., Kirkham, M., DeBell, L., Quine, T.A., Lark, M., Rickson, J., Brazier, R.E., 2017. Testing the utility of structure-from-motion photogrammetry reconstructions using small unmanned aerial vehicles and ground photography to estimate the extent of upland soil erosion. ESPL 42 (12), 1860–1871.

Hosseinalizadeh, M., Kariminejad, N., Campetella, G., Jalalifard, A., Alinejad, M., 2018. Spatial point pattern analysis of piping erosion in loess-derived soils in Golestan Province, Iran. Geoderma 328, 20–29.

Hou, X., Li, R., Jia, Z., Han, Q., Wang, W., Yang, B., 2012. Effects of rotational tillage practices on soil properties, winter wheat yields and water-use efficiency in semi-arid areas of north-West China. Field Crops Res 129, 7–13.

Hu, G., Wu, Y., Liu, B., Yu, Z., You, Z., Zhang, Y., 2007. Short-term gully retreat rates over rolling hill areas in black soil of Northeast China. Catena 71 (2), 321–329.

Huang, C.C., Pang, J., Zha, X., Su, H., Zhou, Y., 2012. Development of gully systems under the combined impact of monsoonal climatic shift and neo-tectonic uplift over the Chinese Loess Plateau. Quat. Int. 263, 46–54.

Jiang, C., Wang, F., Zhang, H., Dong, X., 2016. Quantifying changes in multiple ecosystem services during 2000–2012 on the Loess Plateau, China, as a result of climate variability and ecological restoration. Ecol. Eng. 97, 258–271.

Jones, J.A.A., 1997. The role of natural pipeflow in hillslope drainage and erosion: extrapolating from the maesnant data. PCE 22 (3), 303–308.

Kociuba, W., Janicki, G., Rodzik, J., Stępniewski, K., 2015. Comparison of volumetric and remote sensing methods (TLS) for assessing the development of a permanent forested loess gully. Nat. Hazards 79 (S1), 139–158.

König, H.J., Zhen, L., Helming, K., Uthes, S., Yang, L., Cao, X., Wiggering, H., 2014. Assessing the impact of the sloping land conversion programme on rural sustainability in Guyuan, Western China. Land Degrad. Dev. 25 (4), 385–396.

Li, P., Mu, X., Holden, J., Wu, Y., Irvine, B., Wang, F., Gao, P., Zhao, G., Sun, W., 2017a. Comparison of soil erosion models used to study the Chinese Loess Plateau. Earth-Sci. Rev. 170, 17–30.

Li, X., Jianbing, Peng, Chen, Z., Wang, X., Liu, D., 2003a. Study on tunnel erosion of soil in collapsing loess areas. Research of Soil and Water Conservation 10 (2), 28–32.

Li, Y., Ni, J., Yang, Q., Li, R., 2006. Human impacts on soil erosion identified using land-use changes: a case study from the Loess Plateau, China. PhGeo 27 (2), 109–126.

Li, Y., Poesen, J., Yang, J.C., Fu, B., Zhang, J.H., 2003b. Evaluating gully erosion using 137Cs and 210Pb/137Cs ratio in a reservoir catchment. Soil Tillage Res. 69 (1–2), 107–115.

Li, Z., Liu, W.-z., Zhang, X.-c., Zheng, F.-l., 2009. Impacts of land use change and climate variability on hydrology in an agricultural catchment on the Loess Plateau of China. J. Hydrol. 377 (1–2), 35–42.

Li, Z., Zhang, Y., Zhu, Q., He, Y., Yao, W., 2015. Assessment of bank gully development and vegetation coverage on the Chinese Loess Plateau. Geomo 228, 462–469.

Li, Z., Zhang, Y., Zhu, Q., Yang, S., Li, H., Ma, H., 2017b. A gully erosion assessment model for the Chinese Loess Plateau based on changes in gully length and area. Catena 148, 195–203.

Liu, L., Li, J., Wang, X., 2015. Features on gully erosion and tunnel erosion in loess hilly and gully region. Bulletin of Soil and Water Conservation 35 (1), 14–19.

Liu, X., Wang, F., Yang, S., Li, X., Ma, H., He, X., 2014. Sediment reduction effect of level terrace in the hilly-gully region in the Loess Plateau. J. Hydraul. Eng. 45 (7), 793–799.

Liu, Y., Fu, B., Lü, Y., Wang, Z., Gao, G., 2012. Hydrological responses and soil erosion potential of abandoned cropland in the Loess Plateau, China. Geomo 138 (1), 404–414.

Luo, Y., Yang, S., Liu, X., Liu, C., Zhang, Y., Zhou, Q., Zhou, X., Dong, G., 2015. Suitability of revision to MUSLE for estimating sediment yield in the Loess Plateau of China. Stoch. Environ. Res. Risk Assess. 30 (1), 379–394.

Martínez-Casasnovas, J.A., 2003. A spatial information technology approach for the mapping and quantification of gully erosion. Catena 50 (2), 293–308.

Marzolff, I., Poesen, J., 2009. The potential of 3D gully monitoring with GIS using high-resolution aerial photography and a digital photogrammetry system. Geomo 111 (1–2), 48–60.

Marzolff, I., Ries, J.B., Poesen, J., 2011. Short-term versus medium-term monitoring for detecting gully-erosion variability in a Mediterranean environment. ESPL 36 (12), 1604–1623.

Muhs, D.R., 2018. The geochemistry of loess: Asian and North American deposits compared. JAESc 155, 81–115.

Murray, J.C., Neal, M.J., Labrosse, F., 2013. Development and deployment of an Intelligent Kite Aerial Photography Platform (iKAPP) for site surveying and image acquisition. Journal of Field Robotics 30 (2), 288–307.

Pang, G., Yao, Z., Xie, H., Yang, Q., Li, R., Xie, M., 2013. Soil erosion dynamic changes and its impact factors in Zhifanggou watershed of the Loess Plateau, China. Journal of Food, Agriculture & Environment 11(1), 822–831.

Patton, P.C., Schumm, S.A., 1975. Gully erosion, Northwestern Colorado: a threshold phenomenon. Geology 3 (2), 88–90.

Peng, J., Li, X.a., Fan, W., Chen, Z., 2007. Classification and development pattern of caves in the loess plateau. Earth Sci. Front. 14 (6), 234–244.
Peng, J., Sun, P., Igwe, O., 2018. Loess caves, a special kind of geo-hazard on loess plateau, northwestern China. Eng. Geol. 236, 79–88.
Peter, K.D., d'Oleire-Oltmanns, S., Ries, J.B., Marzolff, I., Ait Hssaine, A., 2014. Soil erosion in gully catchments affected by land-levelling measures in the Souss Basin, Morocco, analysed by rainfall simulation and UAV remote sensing data. Catena 113, 24–40.
Poesen, J., Nachtergaele, J., Verstraeten, G., Valentin, C., 2003. Gully erosion and environmental change importance and research needs. Catena 50 (2), 91–133.
Quan, B., Römkens, M.J.M., Li, R., Wang, F., Chen, J., 2011. Effect of land use and land cover change on soil erosion and the spatio-temporal variation in Liupan Mountain Region, southern Ningxia, China. Front. Environ. Sci. Eng. China 5 (4), 564–572.
Ries, J.B., 2010. Methodologies for soil erosion and land degradation assessment in mediterranean-type ecosystems. Land Degrad. Dev. 21 (2), 171–187.
Ries, J.B., Marzolff, I., 2003. Monitoring of gully erosion in the Central Ebro Basin by large scale aerial photography taken from a remotely controlled blimp. Catena 50 (2), 309–328.
Romero Díaz, A., Marín Sanleandro, P., Sánchez Soriano, A., Belmonte Serrato, F., Faulkner, H., 2007. The causes of piping in a set of abandoned agricultural terraces in Southeast Spain. Catena 69 (3), 282–293.
Selkimäki, M., González-Olabarria, J.R., 2017. Assessing gully erosion occurrence in forest lands in Catalonia (Spain). Land Degrad. Dev. 28 (2), 616–627.
Shi, H., Shao, M., 2000. Soil and water loss from the Loess Plateau in China. J. Arid Environ. 45 (1), 9–20.
Shi, Z.H., Ai, L., Fang, N.F., Zhu, H.D., 2012. Modeling the impacts of integrated small watershed management on soil erosion and sediment delivery: a case study in the Three Gorges Area, China. J. Hydrol. 438-439, 156–167.
Slattery, K.T., Slattery, D.K., Peterson, J.P., 2012. Road construction earthwork volume calculation using three-dimensional laser scanning. J. Surv. Eng. 138 (2), 96–99.
Stöcker, C., Eltner, A., Karrasch, P., 2015. Measuring gullies by synergetic application of UAV and close range photogrammetry — a case study from Andalusia, Spain. Catena 132, 1–11.
Sun, J., 2002. Provenance of loess material and formation of loess deposits on the Chinese Loess Plateau. Earth Planet. Sci. Lett. 203 (3), 845–859.
Sun, W., Shao, Q., Liu, J., Zhai, J., 2014. Assessing the effects of land use and topography on soil erosion on the Loess Plateau in China. Catena 121, 151–163.
Tsoar, H.P.K., 1987. Dust transport and the question of desert loess formation. Sedim 34, 139–153.
Vandaele, K., Poesen, J., Govers, G., Wesemael, B.V., 1996. Geomorphic threshold conditions for ephemeral gully incision. Geomo 16 (2), 161–173.
Vandekerckhove, L., Poesen, J., Govers, G., 2003. Medium-term gully headcut retreat rates in Southeast Spain determined from aerial photographs and ground measurements. Catena 50 (2), 329–352.
Vandekerckhove, L., Poesen, J., Wijdenes, D.O., Gyssels, G., 2001. Short-term bank gully retreat rates in Mediterranean environments. Catena 44 (2), 133–161.
Vandekerckhove, L., Poesen, J., Wijdenes, D.O., Gyssels, G., Beuselinck, L., Luna, E.D., 2000. Characteristics and controlling factors of bank gullies in two semi-arid mediterranean environments. Geomo 33 (1), 37–58.
Verachtert, E., Van Den Eeckhaut, M., Poesen, J., Deckers, J., 2010. Factors controlling the spatial distribution of soil piping erosion on loess-derived soils: a case study from central Belgium. Geomo 118 (3–4), 339–348.
Wang, B.K., 1989. Factors causing tunnel erosion. Acta Soil Water Conserv 3 (3), 84–90.
Wang, Y.Q., Shao, M.A., 2013. Spatial variability of soil physical properties in a region of the Loess Plateau of Pr China subject to wind and water Erosion. Land Degrad. Dev. 24 (3), 296–304.
Wu, Y., Cheng, H., 2005. Monitoring of gully erosion on the Loess Plateau of China using a global positioning system. Catena 63 (2–3), 154–166.
Wu, Y., Zheng, Q., Zhang, Y., Liu, B., Cheng, H., Wang, Y., 2008. Development of gullies and sediment production in the black soil region of northeastern China. Geomo 101 (4), 683–691.
Xin, Z., Yu, X., Lu, X.X., 2011. Factors controlling sediment yield in China's Loess Plateau. ESPL 36 (6), 816–826.
Xu, X., Zheng, F., Wilson, G.V., Wu, M., 2017. Upslope inflow, hillslope gradient, and rainfall intensity impacts on ephemeral gully Erosion. Land Degrad. Dev. 28 (8), 2623–2635.
Zhang, B., He, C., Burnham, M., Zhang, L., 2016. Evaluating the coupling effects of climate aridity and vegetation restoration on soil erosion over the Loess Plateau in China. Sci. Total Environ. 539, 436–449.
Zhang, C., Yang, S., Zhao, C.S., Lou, H., Zhang, Y., Bai, J., Wang, Z., Guan, Y., Zhang, Y., 2018. Topographic data accuracy verification of small consumer UAV. Journal of Remote Sensing 22 (1), 185–195.
Zhang, J.H., Wang, Y., Zhang, Z.H., 2014a. Effect of terrace forms on water and tillage erosion on a hilly landscape in the Yangtze River Basin, China. Geomo 216, 114–124.
Zhang, P., Wei, T., Jia, Z., Han, Q., Ren, X., 2014b. Soil aggregate and crop yield changes with different rates of straw incorporation in semiarid areas of northwest China. Geoderma 230-231, 41–49.
Zhang, P., Wei, T., Li, Y., Wang, K., Jia, Z., Han, Q., Ren, X., 2015. Effects of straw incorporation on the stratification of the soil organic C, total N and C:N ratio in a semiarid region of China. Soil Tillage Res. 153, 28–35.
Zhao, C.S., Zhang, C.B., Yang, S.T., Liu, C.M., Xiang, H., Sun, Y., Yang, Z.Y., Zhang, Y., Yu, X.Y., Shao, N.F., Yu, Q., 2017. Calculating e-flow using UAV and ground monitoring. J. Hydrol. 552, 351–365.
Zhao, G., Mu, X., Wen, Z., Wang, F., Gao, P., 2013. Soil erosion, conservation, and eco-environment changes in the Loess Plateau of China. Land Degrad. Dev. 24 (5), 499–510.
Zhen, L., Cao, S., Cheng, S., Xie, G., Wei, Y., Liu, X., Li, F., 2009. Arable land requirements based on food consumption patterns: case study in rural Guyuan District, Western China. Ecolog. Econ. 69 (7), 1443–1453.
Zhou, J., Shen, R., 2013. Dictionary of Soil Science. Science Press, Beijing.
Zhu, F.S., Rochin, R.I., Chiao, Y.S., 1986. Farming and optimal resource utilization in Guyuan, China. Food Pol 11 (2), 133–142.
Zhu, T.X., 1997. Deep-seated., complex tunnel systems—a hydrological study in a semi-arid catchment, Loess Plateau, China. Geomo 20 (3–4), 255–267.
Zhu, T.X., 2003. Tunnel development over a 12 year period in a semi-arid catchment of the Loess Plateau, China. ESPL 28 (5), 507–525.
Zhu, T.X., 2012. Gully and tunnel erosion in the hilly Loess Plateau region, China. Geomo 153-154, 144–155.
Zhu, T.X., Luk, S.H., Cai, Q.G., 2002. Tunnel erosion and sediment production in the hilly loess region, North China. J. Hydrol. 257 (1–4), 78–90.
Zhu, X.M., 1958. Tunnel erosion in the loess region. Construct. Yellow River 3, 11–15.